Electronic Supplementary Information

Effects of out-of-plane strain and electric fields on the electronic structures of graphene/MTe (M=Al, B) heterostructures

Dingbo Zhang,*[abc] Yue Hu,[a] Hongxia Zhong,[b] Shengjun Yuan [b] and Chang Liu [b]

*Corresponding authors

[a] School of Physical Science and Technology, Key Laboratory of Advanced Technologies of Materials, Ministry of Education of China, Southwest Jiaotong University, Chengdu 610031, China. E-mail: 741220395@qq.com

[b] Key Laboratory of Artificial Micro- and Nano-Structures of Ministry of Education and School of Physics and Technology, Wuhan University, Wuhan 430072, China

[c] Henan Key Laboratory of Photovoltaic Materials, and School of Physics and Materials Science, Henan Normal University, Xinxiang 453007, China

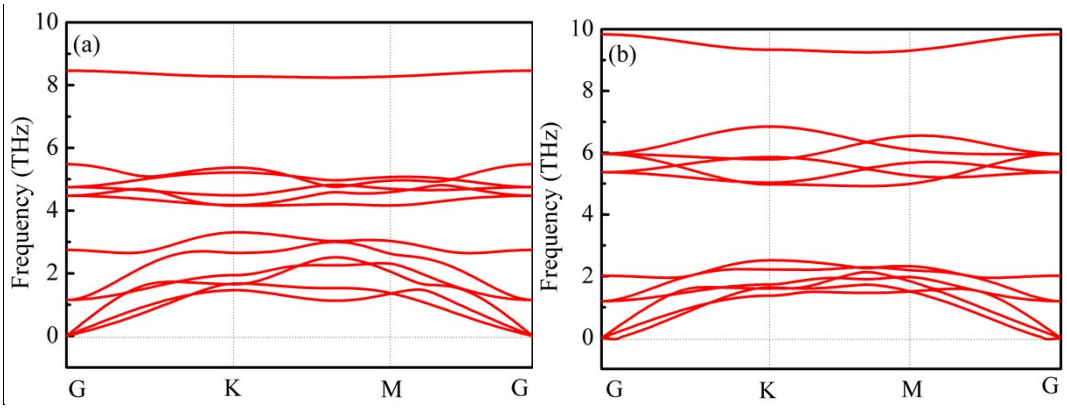

Fig. S1. Phonon spectrums of (a) AlTe and (b) BTe monolayers.

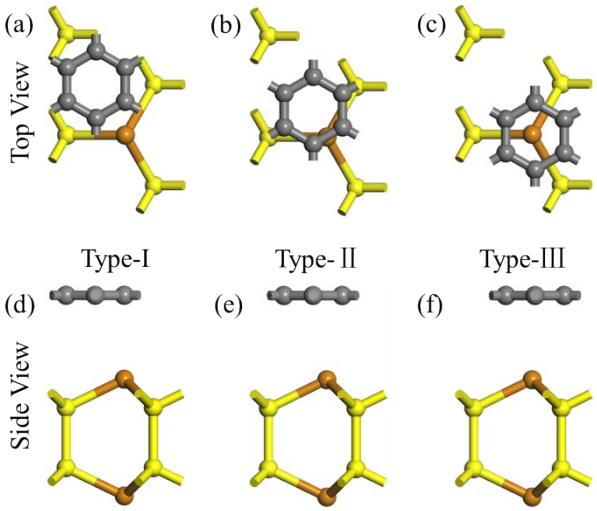

Fig. S2. The stacking patterns type-Ⅰ, type-Ⅱ and type-Ⅲ of graphene/AlTe heterostructures. The gray, yellow and orange balls denote carbon, M and Te atoms, respectively.

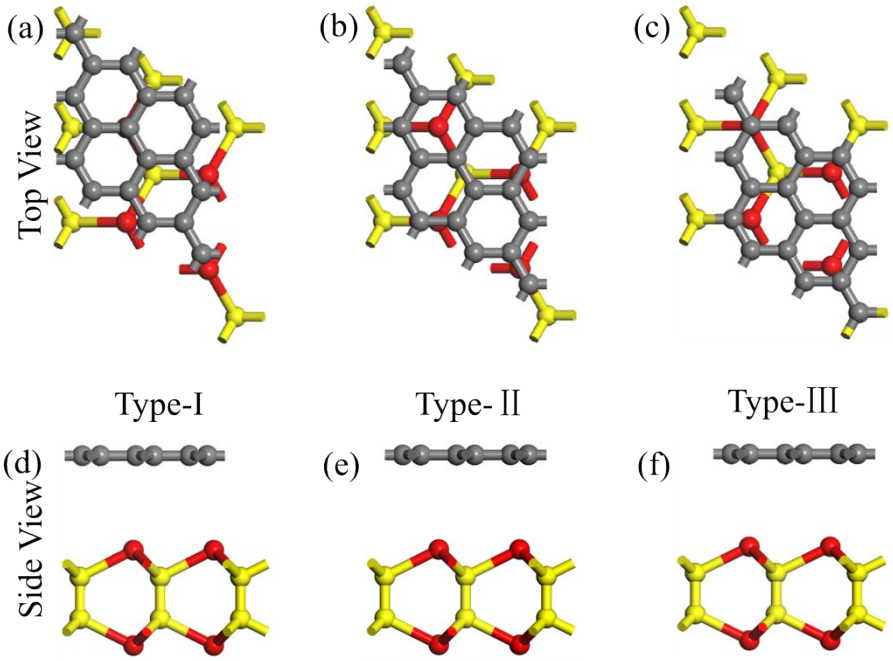

Fig. S3. The stacking patterns type-Ⅰ, type-Ⅱ and type-Ⅲ of graphene/BTe heterostructures. The gray, yellow and red balls denote carbon, M and B atoms, respectively.

Table 1. Optimized lattice constants a=b, binding energies E_b, and interlayer distances D of graphene/MTe (M=Al, B) heterostructures with different stacking configurations.

system	stacking configuration	a=b (Å)	E_b (meV)	D (Å)
graphene/AlTe	type-Ⅰ	4.255	-359.43	3.550
	type-Ⅱ	4.253	-342.31	3.651
	type-Ⅲ	4.250	-339.29	3.656
graphene/BTe	type-Ⅰ	7.270	-150.22	3.673
	type-Ⅱ	7.250	-150.87	3.680
	type-Ⅲ	7.220	-149.93	3.695

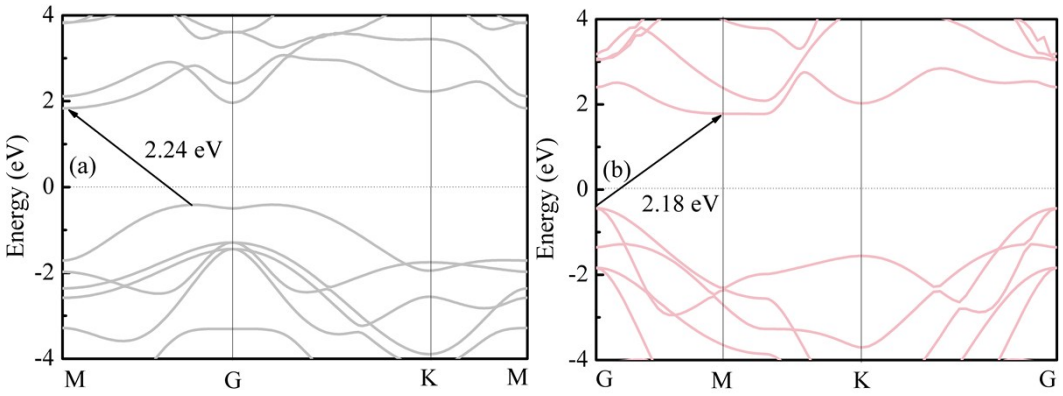

Fig. S4. The band structures of (a) AlTe and (c) BTe calculated using HSE06 method.

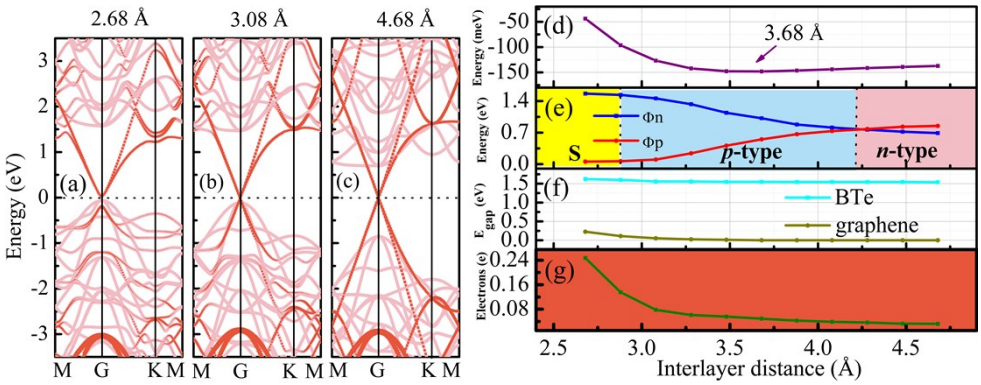

Fig. S5. (a-c) The projected band structures of the graphene/AlTe heterostructures at interlayer distances of D=2.68, 3.08 and 4.68 Å. Orange and magenta symbols represent graphene and AlTe, respectively. (d) The variation of the binding energies, (e) evolution of Schottky barriers, (f) the band gap of garphene and BTe and (g) transferred electrons from the graphene to BTe in the graphene/BTe heterostructures as a function of the interlayer distance.

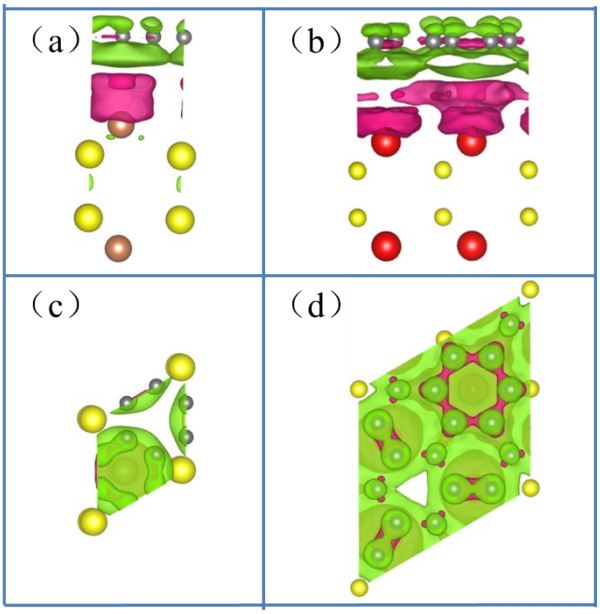

Fig. S6. Differential charge density (a)、(c) of the graphene/AlTe heterostructures at the equilibrium distance. Differential charge density (b)、(d) of the graphene/BTe heterostructures at the equilibrium distance. The lawn-green and deep-pink regions indicate electron decrease and increase, respectively.

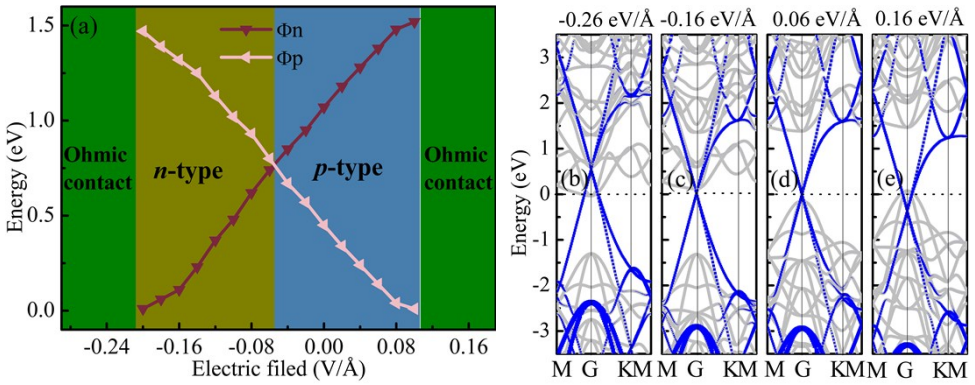

Fig. S7. (a) Schottky barrier Φ_n and Φ_p in the graphene/BTe heterostructures as a function of applying electric fields. (b-e) The projected band structures of the graphene/AlTe heterostructures under applying electric fields of -0.26, -0.16, 0.06 and 0.16 VÅ^{-1}. Orange and magenta symbols represent graphene and AlTe, respectively.

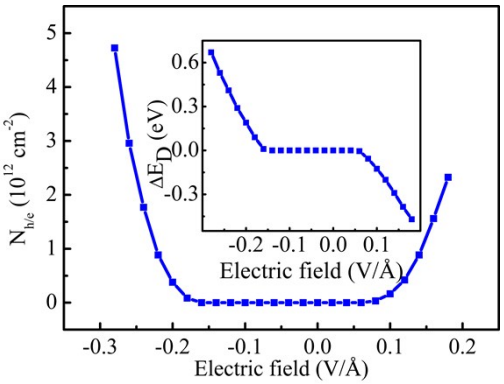

Fig. S8. The doping charge carrier concentration $N_{h/e}$ (10^{12} cm^{-2}) as a function of applying electric fields in the graphene/AlTe heterostructures. The difference ΔE_D between Dirac point of grahene and the Fermi level is plotted in the inset.